Critical current studies of a superconducting square coil

Z. Zhong,[1, a)] M. Chudy,[2, b)] H. S. Ruiz,[1] X. Zhang,[1] and T. Coombs[1]
[1)] *Department of Engineering, University of Cambridge.*
[2)] *Graduate School of Technology Management, University of Pretoria*

(Dated: 25 May 2015)

Nowadays, many high-field magnets take advantage of the superior properties of superconductors. The superconducting square coil, a promising alternative for building Helmholtz coil has aroused great interest. This paper focuses on the critical current angular dependence of a superconducting square coil. The critical current of the entire coil and two selected strands under different magnitudes and orientations of external magnetic fields have been measured. The critical regions of the coil in different angular regimes were determined. A better understanding of the in-field performance of superconducting square coil is obtained.

PACS numbers: JD15-4615

I. INTRODUCTION

The high and lossless current-carrying capability of superconductors has been widely recognized. Nowadays, many high-field magnets take advantage of the superior properties of superconductors[1]. To achieve a compact design for superconducting applications, superconductors are wound into different types of coils. Two of the most common coil shapes are pancake coils and racetrack coils. Pancake coils are circular bifilar coils that contain two closely-spaced, parallel windings. The name "racetrack" coil arises because at each end the superconductor loops around 180° like the end of a race track. Pancake coils wound using HTS are a viable design option for spatially homogeneous magnets such as NMR and MRI magnets[23]. Racetrack coils, on the other hand, are preferred in generators[4], motors[5], and maglev systems[6].

Most superconducting coil based applications involve external magnetic fields or background fields, which are large enough to significantly affect the critical current of a superconducting coil. In addition, the anisotropic nature of superconducting tape has a great impact on the in-field performance of superconducting coils. Many numerical methods have been proposed to study the behaviour of superconducting coils. Critical regions and sub-critical regions were assumed by J.R. Clem[7], depending on the magnetic environment. W. Yuan[8] predicted the boundary between these two regions by using a parabolic function and calculated the current distribution within the sub-critical regions. V.M.R. Zerme*ñ*o[9] made a further step towards efficient modelling by devising a 3D approach.

Some experimental studies have also been carried out. The field angular dependence of a racetrack coil has been measured, in which the critical current variation showed a good agreement with that of a single tape[10]. The critical current for different radial parts (from inner sections to outer sections) of a pancake coil has also been measured, suggesting that the inner layers contribute much more to the resulting end-to-end voltage drop than the outer layers do, when the applied current is greater than a critical value. This could jeopardize the smooth operation of a superconducting coil. As a result, a more adequate criteria for determining the critical current of a superconducting coil was proposed[11].

Rapid developments have been made in superconducting coil fabrication processes and technology[12]. Initially, the dry winding technique was widely used, which wound superconducting coil without any filler material. The main drawback of this technique is the motion and friction of the conductor within the coil windings caused by the Lorentz force, even though global winding motions can be controlled over a macroscopic scale by mechanical reinforcement. However, the heat generated by conductor motion can be effectively taken away by cryogenic coolant irrigation of the porous windings[13]. Coil based superconductors can therefore be safely used for most purposes[14]. Impregnation of coil windings with filler materials is an alternative approach. The material fills the winding voids and thereby prevents the Lorentz force-induced conductor motion. Materials with low moduli of elasticity have been used and evaluated as impregnates, and epoxy resin was proven to be the most successful candidate. However, this is by no means a flawless solution, as the critical current of an epoxy-impregnated YBCO coil can be substantially degraded[1516]. Currently there is no standard way of producing superconducting coils and the most desired solution is usually realized based on case-specific analysis.

Recently, a new type of superconducting coils, the square coil, has aroused great interest. For a Helmholtz coil, they have been proven to be better candidates than circular windings in generating a more uniform magnetic field[17]. However, this geometry also results in a concentration of the coil self-field in certain regions. Investigation into the field distribution is required. The situation becomes even more complicated if a square coil is in the presence of an external magnetic field. At present, few studies have been done with respect to a square superconducting coils. A deep insight into the factors that determine the critical current of square coils would be

[a)] Electronic mail: zz272@cam.ac.uk
[b)] Also at Department of Engineering, University of Cambridge.

extremely beneficial.

Some extra care needs to be taken while fabricating square superconducting coils. First, the corners have to be made circular with a diameter greater than that of the minimum bending diameter of the winding tapes. Second, as superconductor wires pass around a corner, the tape cannot easily be bound to the straight parts of the frame. Gaps are more likely to exist between the innermost layer of the coil windings and the frame. This gap, although small, could still have a large influence on the overall performance of a square coil.

This paper measures the field angular dependence of the critical current for two selected sections of a square coil as well as for the entire coil. The effect of flux cutting and flux transport (de-pinning) on the critical current of selected sections and the entire coil are discussed. The effects of mechanical disturbance induced by the small gaps are investigated. The critical region that dominates the overall critical current of the coil is identified in different angular regimes.

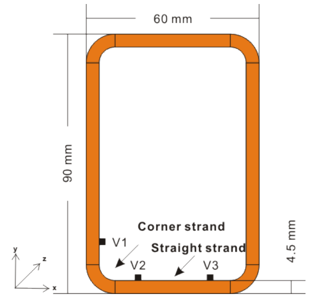

(a) Dimension drawing of the square coil.

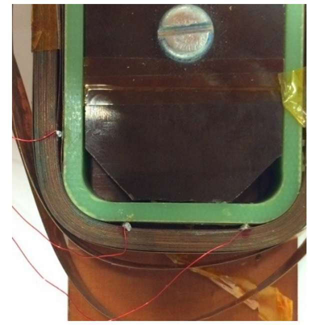

(b) Picture of the square coil.

FIG. 1: Dimension drawing and picture of the square coil. It can be seen in Figure 1b that a small gap exists between the innermost layer of the straight strand and the G10 frame.

II. EXPERIMENTAL PROCEDURE

A. Test Coil

A square coil was wound using Superpower® SCS6050 tape[18], which is a double stack rectangular-shaped 2G HTS coil. Kapton® tapes were used as electrical isolation between turns. The dimensions of the coil are illustrated in Figure 1a. Several parameters of the superconducting coil are collected in Table I.

Voltage taps were soldered to the terminals at each end of the coil to evaluate the critical current of the entire coil. Three additional voltage taps (V1, V2, and V3) were also soldered to the straight portion and corner portion of the innermost layer, spacing 25 mm from each other, to determine the critical current of the corresponding strands (see Figure 1). The straight strand, where voltage taps V2 and V3 were accommodated, was not bound to the frame. The maximum distance between the innermost layer of the straight strand and the frame was measured to be 1.4 mm. Windings in other regions were bound to the G10 frame using Kapton® tapes.

TABLE I: Parameters of the superconducting coil

Tape type	Superpower® SCS6050 (crica 2013)
Tape width	6 mm
Tape thickness	100 μm
Substrate	50 μm Hastelloy® C-27, non-magnetic
Number of turns	32 turns per layer (two layers)
Length	16.6 m
Critical current	66 A (self-field)

The coil was mounted on a tufnol support board, together with all the sensors and instrument wires. Each terminal was connected to the current lead by clamping it between two copper plates. A Hall probe was placed at the centre of the coil to monitor the magnitude of the magnetic fields.

B. Experimental set-up

A schematic drawing of the experimental set-up is displayed in Figure 2. Transport I_c measurements of the entire coil and selected sections were performed using a four-probe technique and an electric field criterion of $E_0{=}1\times10^{-4}$ V/m. The coil was completely immersed in a liquid nitrogen bath. The applied current was ramped up at 2 As^{-1} to reduce the impact of inductance inside the coil. Angular studies were performed in an electromagnet with a field homogeneity of 8% ppm in the region where the test coil was placed. The maximum achievable field is 330 mT for this air-gap. The magnetic field was monitored by a Hall sensor placed at the centre. The coil was rotated by a high precision manual rotation stage (graduation of 1° and vernier of 5′) around a vertical axis. An Agilent 6680A was used as the current source and two Keithley 2182 nanovoltmeters were employed to monitor the voltage signals of the entire coil as well as the selected sections. The measurements were controlled using a LabVIEW platform.

III. RESULTS AND DISCUSSION

The critical current measurement in the self-field condition was first performed, giving a critical current of 66 A for the entire coil, 63 A for the straight strand and 58 A for the corner strand, respectively. The second innermost layer was chosen for characterization as the innermost layer contains a crossover of the tapes between the windings. The I_c of the coil was higher than for the innermost strands. This occurs because I_c is determined

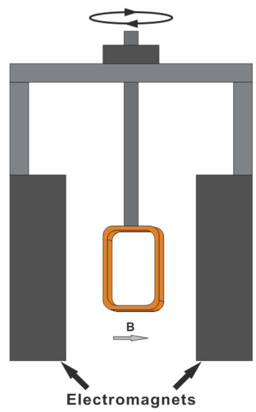

FIG. 2: Experimental Set-up

as being when E>E_0. When E>E_0 for the entire coil, the electric field (E) of the innermost strands is considerably higher than E_0[11]. The variation of the critical currents in different regions could be attributed to either one or both of the effects of the inhomogeneous field distribution and different mechanical conditions experienced by the straight and corner strands. These two factors are discussed in section III A and section III B.

The critical current was then measured in the presence of external magnetic fields with various magnitudes. The angle between **H** and the coil is defined as $\theta_{coil} = 0°$ when the external field is perpendicular to the x-y plane (see Figure 1a), and the coil was rotated clockwise around the y axis with an interval of 4 degrees. The critical current of either the corner strand or straight strand could not be determined under all conditions, such as the angular regions that are close to 0° under higher external magnetic fields. This is due to the protection mechanism applied. The transport current was regulated to zero when a pre-set threshold voltage for the entire coil (6 mV) was exceeded, while the voltages of either corner and straight strands remained well below the criteria voltage V_c of 2.5 μV (see Figure 3).

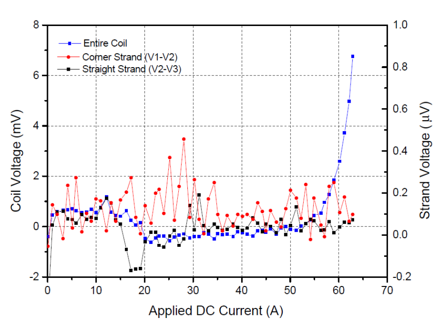

FIG. 3: The test coil was subjected to a 200 mT external magnetic field, θ_{coil}=0°.

A. Inhomogeneous magnetic field distribution

Superconducting strands in the innermost layer tend to experience the highest density of the magnetic self-field generated by the coil, and therefore are penetrated more by the critical regions compared to the outer turns, leading to a lower critical current[19]. Unlike circular-shape pancake coils, where each layer of a superconducting coil enjoys a similar magnetic field condition, every single part of a rectangular-shaped coil, can experience different densities and orientations of magnetic fields. Due to the effects of geometry, the corners of the innermost layer are in the presence of the strongest field in self-field conditions. A Comsol model (see Figure 4) shows that the corner regions and inner layers experience stronger magnetic fields than the straight portions and outer layers. A peak magnetic flux density of 0.24 T is present at one corner of the innermost layer, while a minimum of 0.129 T is seen at one corner of the outermost later when an external current of 69 A is applied. The average flux density along the straight strands is smaller than that of the corner strands in each layer. This could be due to the field superposition at the corner regions. Thus, a lower critical current is expected at the corner strand than in the straight strand in the self-field condition.

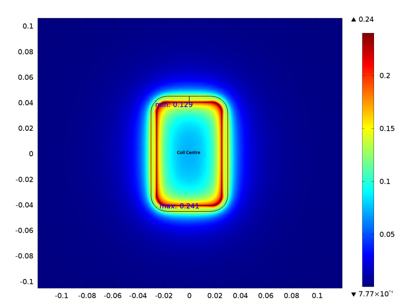

FIG. 4: Magnetic flux density (T) at the center-cut plane of the coil, when an external current of 66 A is applied.

The situation becomes more complicated when an external magnetic field is applied, that is, the field distribution is more complex because of the vector superposition of the applied magnetic fields and the self-field generated by the coil. The strongest magnetic field may occur in any region in a given field orientation and magnitude. The peak field is no longer confined to the innermost layer, nor to any other specific region. The field distribution changes greatly as the orientation of the applied fields varies. Another important issue which needs to be addressed is the field orientation. Different field angles are defined depending on the direction of the rotation: the tilt angle and the rotation angle. The definition of these two angles is illustrated in Figure 5. θ is defined as 0° when $H \parallel c$ axis, and 90° when $H \parallel ab$ plane. φ is defined as 0° when the sample is subject to the maximum Lorentz force configuration, and 90° when the sample is subject to the minimal Lorentz force configuration (i.e. the applied field is parallel to the current direction.). When the coil is rotated around the y axis as shown in Figure 6, the superconducting strands in the straight part A (coloured in blue) are always in the maximal Lorentz force configuration, in which the orientation of the applied magnetic field is always perpendicular to the current direction. A characteristic curve for the angular dependence of the critical current on the applied magnetic field was obtained for SuperPower samples (see Figure 7).

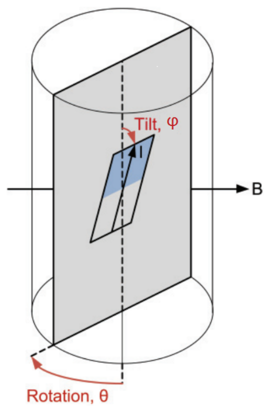

FIG. 5: The definitions of the rotation angle (θ) and the tilt angle (φ).

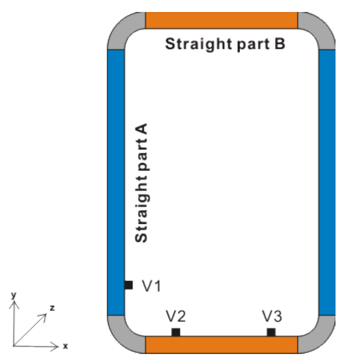

FIG. 6: The coil is divided into three parts depending on various field conditions experienced. The y-axis runs through the centre of the coil.

A different situation occurs for the straight part B (coloured in orange Figure 6). In these parts, the superconducting strands experience an in-plane magnetic field (the x-z plane as shown in Figure 6). During rotation, it is expected that B_z will not have a great influence on the critical current, due to the strong intrinsic pinning arising from the layered structure. B_x, on the other hand, is parallel to the current direction. The enhancement of the critical current caused by this parallel component of an applied magnetic field has been observed[22,23,24]. Flux cutting is believed to be responsible for this enhancement[25,26]. A general critical state model

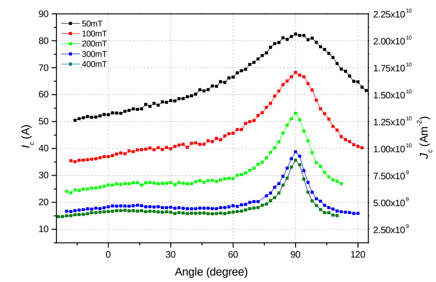

FIG. 7: Critical current of 4 mm wide Superpower® samples as a function of magnetic field orientations at 77 K. 0° is defined as when the applied field is perpendicular to the broad surface of the sample, and defined as 90° when the applied field is parallel to the broad surface of the sample.

(GCSM) that could describe this phenomenon was first proposed by Clem[27,28], which takes into account both vortex motions induced by transverse current and vortex twist caused by longitudinal currents. This model is purely phenomenological. Campbell[29] admits that "we are a long way from even a qualitative understanding of flux cutting and longitudinal currents." The intricate flux cutting theory will therefore not be explored in this paper, instead, we focus on the enhancement of critical current of a superconducting strand when it is in the presence of longitudinal applied fields, and the effects on the entire square coil.

The critical current dependence of a superconducting tape on in-plane applied fields has been studied previously[24,20]. It can be seen from Figure 8a that the critical current is not sensitive to a moderate tilt angle ($\varphi < 45$ °), whilst increases remarkably at higher tilt angles. The peaks are seen at $\varphi = 90°$ (force-free configuration) when the applied field is perpendicular to the sample surface ($H \parallel c$). The critical current remains level with the variation in tilt angle when the applied field is parallel to the sample surface, where **H** is always parallel to the ab plane and perpendicular to **I**. The magnetic field component that is perpendicular to the current direction therefore does not exert a great influence on the performance of the critical current.

The fan-shaped corner strand (coloured in grey in Figure 6), experiences various tilt angles in a broad range of tilt angles from 0° to 90° at certain rotation angles. Figure 8b shows the I_c variations depending on both rotation angle and tilt angle. When the tilt angle is smaller than 45°, the rotation angle determines the critical current. Only a minute I_c enhancement is observed, whereas the value of the sharp maximum seen at a rotation angle of 90° remains unchanged. As the applied field progressively tilts to a direction aligned to the direction of current **I**, a pronounced I_c enhancement is achieved for all rotation angles apart from 90° and 270°. A completely different tendency is seen in the critical current profiles when $\varphi = 90°$. This occurs when an in-plane field is applied to the sample, so that the rotation angle θ essentially represents the angle between $\mathbf{B}$ and $\mathbf{I}$. A minimum is seen when $\mathbf{B} \perp \mathbf{I}$, while a maximum is seen when $\mathbf{B} \parallel \mathbf{I}$.

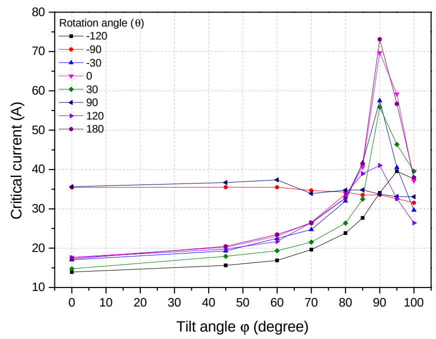

(a) Critical current vs. tilt angles (φ).

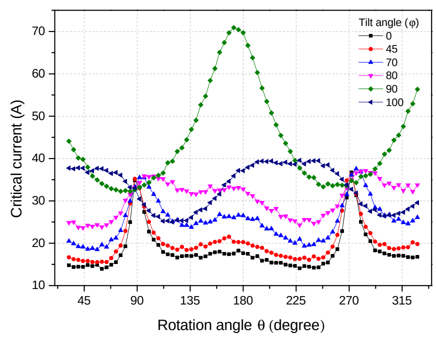

(b) Critical current vs. rotation angles (θ).

FIG. 8: Two-axis orientation dependent critical current measurements on a SuperPower® sample. The conductor was subjected to an applied magnetic field of 500 mT.

B. Mechanical strain and conductor motions

The interaction between magnetic fields and transport current causes a variation in the Lorentz force exerted on different superconducting strands. This force generally leads to tensile strain, which can influence the performance of a superconductor[30,31]. Investigations into the relationship between the critical current and strain/stress have been done by Hyung-Seop Shin[32], and show that I_c experiences a slight increase, reaching a peak at a strain of $\varepsilon_{irr.}$=0.25%. I_c begins to degrade rapidly with a further increase in strain. The critical axial tensile stress reported by the manufacturer is 4.5%[33], which is far beyond the tensile stress experienced by the measured coil. Thus, the effect of tensile strain is negligible. Another type of deformation is bending, which also leads to I_c degradation[34]. However, the bend diameter for this square coil is (24 mm), which is substantially larger than the critical tensile bend diameter (11 mm) reported by the manufacturer[33], and therefore should not cause any I_c reduction for this coil.

The air gap between the innermost layer of the straight part B and the G10 support frame (see Figure 1b and Figure 9) can have a deep influence on the critical current of corresponding strands in the presence of external magnetic fields. The air gap either expands or contracts due to the Lorentz force exerted. The force F_l can be calculated as:

$$\mathbf{F}_l = I \int dl \times \mathbf{B} \tag{1}$$

The average force exerted on the 25 mm long straight strand (innermost layer) is estimated by a simulation performed using Comsol 4.4b, the results of which are presented in Figure 10. The direction of the self-field is opposite to direction of the applied field at $\theta_{coil} = 0°$. This is defined as positive when the resulting Lorentz force is in the -y direction as illustrated in Figure 6. Figure 10 shows that at $\theta_{coil} = 135°$ and $\theta_{coil} = 225°$, the straight strand experiences approximately the same force in the y direction under different magnitudes of applied magnetic field. Therefore, similar conductor movement is expected for the strand at these two coil rotation angles for different applied fields.

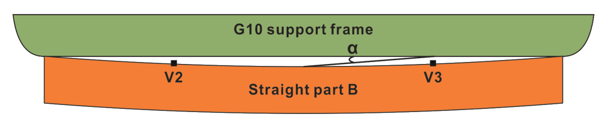

FIG. 9: Schematic illustration for the bottom section of the measured square coil (refer to Figure 1b). The maximum distance between the innermost layer of straight part B and the G10 support frame is 1.4 mm. α is estimated to be 6°.

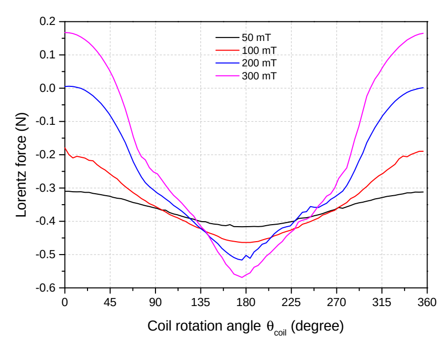

FIG. 10: Simulation results for the Lorentz force exerted on the 25 mm long straight strand (innermost layer).

As the bottom straight part B was left loose, the magnitude of the Lorentz force is sufficient to push the strands upwards in the +y direction, especially in the presence of strong fields (200 mT, 300 mT). Therefore, the x component of the applied field (B_x) is no longer always aligned with the current direction ($\mathbf{I}$). Instead, there is a slight tilt between B_x and $\mathbf{I}$, with various angles over different regions of the curved strands. Though the tilt angles are small (<10°), they tend to affect the critical current significantly (see Figure 8b). According to Figure 5, $\mathbf{B}$ is an in-plane applied field when tilt angle φ= 90°. Figure 8b shows that the critical current of a single tape is extremely sensitive to a slight 'off-plane' tilt. A completely different picture is seen for φ= 80° and φ= 100° compared to φ= 90°. It is essentially the case for the left half and right half of the straight part B (see Figure 9). Either the left half or the right half could be the critical region for the straight part B, depending on the coil rotation angle (θ_{coil}), and determine the critical current for the entire strand.

C. Critical current for different sections of the measured square coil

Critical currents for the straight strand (straight part B), the corner strand and the entire coil were measured under four different magnitudes of applied magnetic fields: 50 mT, 100 mT, 200 mT, and 300 mT. Applied field magnitudes could be distinguished into three levels: moderate fields where the applied field is smaller than the coil self-field (e.g., 50 mT); intermediate fields where the applied field is comparable to the coil self-field (e.g., 100 mT); and strong fields where the applied field is greater than twice that of the self-field (e.g., 200 mT and 300 mT). The critical current profiles are presented in Figure 11. As the critical current of the entire coil was evaluated using the end-to-end voltage, it is essentially the overall average for each part of the coil. Therefore, some parts or layers can contribute more to the resulting end-to-end voltage than others, in which case the corresponding part or layer becomes the predominant factor in determining the critical current of the entire coil.

Now we try to identify the critical regions for the sample square coil when in the presence of an external magnetic field of varying angles. As mentioned previously, the square coil is divided into three parts. It is expected that a given part within each superconducting layer experiences a similar field orientation but varying field magnitudes. The innermost layer of one part can therefore serve as a representative to study the critical current tendency of a corresponding part. In the experiments, the square coil was rotated around the y-axis, and the rotation angle of the coil (θ_{coil}) is defined as 0° when the applied field is perpendicular to the x-y plane (see Figure 6). Thus, the applied field is perpendicular to the ab-plane of the superconducting strands in the straight part A when $\theta_{coil} = 0°$, and is an in-plane applied field with $\mathbf{B} \perp \mathbf{I}$ for the straight part B.

The critical current variation of the straight strand (bottom straight part B) decreases monotonically as the applied field progressively tilts towards the direction of the flowing current. A minimum is reached at 135°. Then the critical current experiences a gentle increase for all of the remaining angular regions when a 50 mT external field is applied (see Figure 11a). For intermediate and strong fields, the critical current begins to decrease after reaching a smaller peak at $\theta_{coil} = 180°$, arriving at another minimum at 225° (see Figure 11b, Figure 11c and Figure 11d), and rising again with a further increase in coil rotation angle. The tendency is far from what was expected. If the straight strand is closely bonded to the frame, so that the applied field is always in-plane, the critical current is expected to reach peaks at 90° and 270° where $\mathbf{B}$ is aligned with $\mathbf{I}$, and reach minimums at 0°, 180° and 360°, when $\mathbf{B}$ is perpendicular to $\mathbf{I}$[23,22]. However, this straight strand was not tightly bound, and a small gap was seen between the straight strand and the G10 frame (see Figure 1b). Therefore, this straight strand was slightly curved and experienced a small 'off-plane' tilt field instead. Figure 11 shows that this small conductor motion has a great impact on the resulting critical current curve. As shown in Figure 10, the Lorentz force exerted on the straight strand is approximately the same under applied fields of different magnitudes at $\theta_{coil} = 135°$ and $\theta_{coil} = 225°$, suggesting similar conductor movement. Therefore, the minimum values for the straight strand critical current at these two angles possibly result from the joint action of conductor motion and 'tilting' of the applied magnetic fields. However, wire motions are expected to be insignificant for the entire straight part B because all the other parts were tightly bonded to the frame.

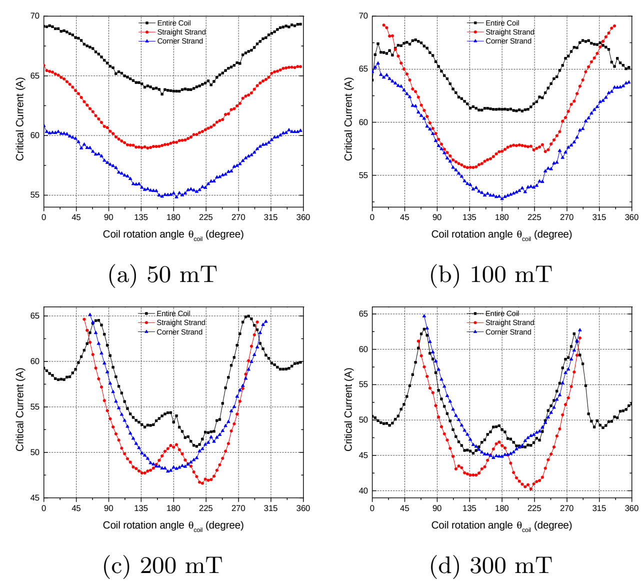

(a) 50 mT (b) 100 mT

(c) 200 mT (d) 300 mT

FIG. 11: Critical current for the corner strand, the straight strand, and the entire coil under various field magnitudes and orientations.

Figure 11a shows that the critical current variation of the corner strand and the entire coil are identical under a

50 mT external magnetic field, suggesting that the corner areas are the critical region for all rotation angles under moderate fields ($\leq$ 50 mT). This could be due to the fact that the self-field of the superconducting coil is concentrated in the corner regions, whereas the applied field is too small to become a major factor. When the applied field is 100 mT, in the angular regions where 135 $<\theta_{coil}$ $<$225, the critical current of the entire coil remains level, which may have originated from compensation between the straight strand and the corner strand. The straight part A is not considered to play an important role in determining the overall critical current, as the critical current variation is expected to be moderate in the angular regime (see Figure 7). The situation becomes different when stronger fields are applied (200 mT and 300 mT), where the straight strand dominates the overall critical current of the coil. The crossings between the critical current of the straight strand, the corner strand and the entire coil indicates that for θ_{coil} $<$80° and θ_{coil} $>$280°, the innermost layer is no longer the critical region in determining the overall critical current under strong fields.

Figure 13 shows the critical current variation of the entire coil. As discussed before, the overall critical current is mainly determined by the corner part when the applied field is low (50 mT and 100 mT). However, in the case of a strong applied field, straight part A and straight part B turn into major factors. As mentioned previously, the straight part B as a whole is not expected to be significantly affected by the wire motion since all the other parts of the wire were reinforced. The in-plane applied magnetic field is therefore considered to be the primary factor in determining the critical current for the whole part. The critical current variation of each part with respect to field orientation should be similar to that of a single tape. Figure 12b presents a schematic diagram showing the expected tendency of critical current for the straight part A and the straight part B. When θ_{coil} = 0°, the applied field, B_{app} is in the z direction when the current flows in the x-y plane (see Figure 12a).

Figure 12b shows that the critical current decreases much faster in the angular regime 0$<\theta_{coil}<$45 than in 45$<\theta_{coil}<$90 in straight part A. In straight part B, the critical current increases more rapidly in the angular regime 45$<\theta_{coil}<$90 than in 0$<\theta_{coil}<$45. The changing slope of the critical current over different angular regimes leads to the presence of multiple peaks and minimums for the critical current of the entire coil (see Figure 13). The critical current reduction for the straight part A is much greater than the increase for the straight part B for 0$<\theta_{coil}<$45, and therefore the critical current for the entire coil experiences a reduction in the critical current. For the angular regime 45$<\theta_{coil}<$90, the large critical current increase in the straight part B and slight decrease in the straight part A result in an increase in the critical current of the entire coil. A similar explanation applies to all the remaining angular regimes. Therefore, we have identified that the angular regimes in which either the straight part A or the straight part B take a dominant

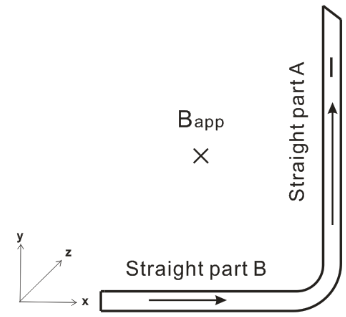

(a) Illustration of the current and field directions for the coil at $\theta_{coil} = 0°$. The cross indicates that the applied field is in the z direction. The arrows indicate the direction of the current.

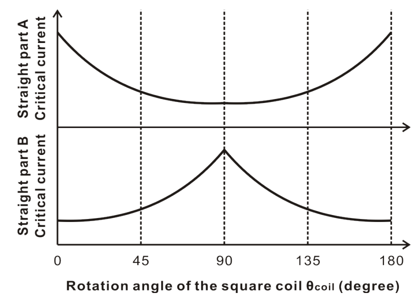

(b) Expected trends of critical currents for the straight part A and straight part B according the experiments performed on a single tape.

FIG. 12: Illustration of the current and field directions for part of the coil at $\theta_{coil} = 0°$, and expected trends of critical current for the straight part A and straight part B with respect to the coil rotation angle, θ_{coil}. The tendency was estimated according to the experimental results from a single tape (see Figure 7 and Figure 8a).

role in determining the critical current of the entire coil in the presence of a strong applied field: the straight part A dominates when 0$<\theta_{coil}<$45, 135$<\theta_{coil}<$225 and 315$<\theta_{coil}<$360. And the straight part B dominates when 45$<\theta_{coil}<$135 and 225$<\theta_{coil}<$315.

The critical current of the entire coil was determined using the end-to-end voltage, which is essentially the integration of the electric field over the length of the sample. The straight part A (80 mm) is longer than straight part B (50 mm), and therefore contributes more to the end-to-end voltage, providing that a similar electric field is experienced by both parts. This is the reason why the peaks and minimums shown in Figure 13 shift to the angular regimes where the critical current of the straight part A experiences a rapid increase or decrease.

IV. CONCLUSION

The in-field critical current performance of a square coil is studied. The critical currents of the entire coil

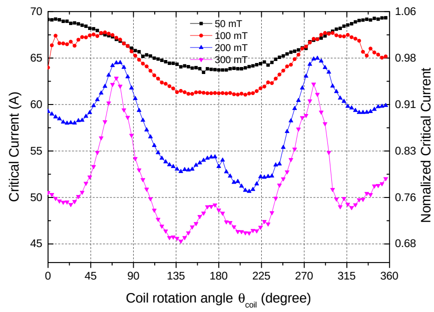

FIG. 13: Critical current of the entire coil subjected to different external fields. I_c is normalized to the self-field values to better demonstrate the comparison.

and two selected strands under different magnitudes and orientations of external magnetic field are acquired. A small gap between the innermost layer and the frame can have a huge impact on the critical current for the innermost layer. Therefore, it is advisable to impregnate a square coil to reduce wire motions. Corner regions are considered to be the critical region for a square coil in the presence of a small or intermediate external magnetic field, the magnitude of which is smaller or comparable to the self-field generated at the centre of the coil. In the case of a strong magnetic field, either the straight part A(longer portion) or the straight part B(shorter portion) can become the dominant factor in determining the critical current of the entire coil in certain angular regimes.

[1] A. M. Asner, *High field superconducting magnets* (Clarendon Press, 1999).
[2] J. Bascuñán, H. Lee, E. S. Bobrov, and Y. Iwasa, "A low- and high-temperature superconducting nmr magnet: Design and performance results," Applied Superconductivity, IEEE Transactions on **13**, 1550–1553 (2003).
[3] B. C. Breneman, R. E. Sarwinski, and Y.-H. L. Hsu, "Superconducting mri magnet with magnetic flux field homogeneity control," (1993), uS Patent 5,194,810.
[4] H. Wen, W. Bailey, K. Goddard, M. Al-Mosawi, C. Beduz, and Y. Yang, "Performance test of a 100 kw hts generator operating at 67 k–77 k," Applied Superconductivity, IEEE Transactions on **19**, 1652–1655 (2009).
[5] Z. Huang, W. Xian, M. Zhang, M. Chudy, Y. Chen, Z. Zhong, M. Baghdadi, W. Wang, F. Spaven, K. Matsuda, *et al.*, "Control and operation of a high temperature superconducting synchronous motor," Applied Superconductivity, IEEE Transactions on **23**, 5200204–5200204 (2013).
[6] K. Tasaki, K. Marukawa, S. Hanai, T. Tosaka, T. Kuriyama, T. Yamashita, Y. Yanase, M. Yamaji, H. Nakao, M. Igarashi, *et al.*, "Hts magnet for maglev applications (1) coil characteristics," Applied Superconductivity, IEEE Transactions on **16**, 1100–1103 (2006).
[7] J. R. Clem, J. Claassen, and Y. Mawatari, "Ac losses in a finite z stack using an anisotropic homogeneous-medium approximation," Superconductor Science and Technology **20**, 1130 (2007).
[8] W. Yuan, T. Coombs, J.-H. Kim, C. H. Kim, J. Kvitkovic, and S. Pamidi, "Measurements and calculations of transport ac loss in second generation high temperature superconducting pancake coils," Journal of Applied Physics **110**, 113906 (2011).
[9] V. M. Zermeño and F. Grilli, "3-d modeling and simulation of 2g hts stacks and coils," arXiv preprint arXiv:1311.3580 (2013).
[10] M. Chudy, Y. Chen, M. Zhang, and T. Coombs, "Anisotropy of 2g hts racetrack coils in external magnetic fields," Superconductor Science and Technology **26**, 075012 (2013).
[11] M. Zhang, J.-H. Kim, S. Pamidi, M. Chudy, W. Yuan, and T. Coombs, "Study of second generation, high-temperature superconducting coils: Determination of critical current," Journal of Applied Physics **111**, 083902 (2012).
[12] Y. Iwasa, *Case studies in superconducting magnets: design and operational issues* (Springer, 2009).
[13] J. Williams, "High current density superconducting coils," Tech. Rep. (Massachusetts Inst. of Tech., Cambridge (USA). National Magnet Lab., 1967).
[14] Y. Iwasa, "Experimental and theoretical investigation of mechanical disturbances in epoxy-impregnated superconducting coils. 1. general introduction," Cryogenics **25**, 304–306 (1985).
[15] T. Takematsu, R. Hu, T. Takao, Y. Yanagisawa, H. Nakagome, D. Uglietti, T. Kiyoshi, M. Takahashi, and H. Maeda, "Degradation of the performance of a ybco-coated conductor double pancake coil due to epoxy impregnation," Physica C: Superconductivity **470**, 674–677 (2010).
[16] D. Van Der Laan, J. Ekin, C. Clickner, and T. Stauffer, "Delamination strength of ybco coated conductors under transverse tensile stress," Superconductor Science and Technology **20**, 765 (2007).
[17] U. Prasad, A. Amardas, D. Patel, S. Pradhan, *et al.*, "Design and fabrication of a high t_c bscco based square helmholtz coil," in *Journal of Physics: Conference Series*, Vol. 208 (IOP Publishing, 2010) p. 012021.
[18] superpower, "superpower tape description," (2013).
[19] M. Zhang, J. Kvitkovic, C. Kim, S. Pamidi, and T. Combs, "Study of 2g high temperature superconducting coils: Influence of anisotropic characteristics," Journal of Applied Physics **114**, 043901 (2013).
[20] S. Hopkins, M. Woźniak, B. Glowacki, Y. Chen, I. Kesgin, and V. Selvamanickam, "Two-axis magnetic field orientation dependence of critical current in full-width rebco coated conductors," Physics Procedia **36**, 582–587 (2012).
[21] M. Chudy, Z. Zhong, M. Eisterer, and T. Coombs, "n-values of commercial ybco tapes before and after irradiation by fast neutrons," Superconductor Science and Technology **28**, 035008 (2015).
[22] E. H. Brandt and G. Mikitik, "Longitudinal magnetic field increases critical current in superconducting strip," in *Journal of Physics: Conference Series*, Vol. 150 (IOP Publishing, 2009) p. 052024.
[23] G. P. Mikitik and E. H. Brandt, "Vortex shaking in rectangular superconducting platelets," Physical Review B **69**, 134521 (2004).
[24] M. Chudỳ, S. Hopkins, M. Woźniak, B. Glowacki, M. Eisterer, and H. Weber, "Full angular critical current characteristics of coated conductors studied using a two-axis high current goniometer," Superconductor Science and Technology **24**, 075018 (2011).
[25] V. Vlasko-Vlasov, A. Koshelev, A. Glatz, C. Phillips, U. Welp, and W. Kwok, "Flux cutting in high-t_c superconductors," Physical Review B **91**, 014516 (2015).
[26] L. Fisher, K. Il'enko, A. Kalinov, M. LeBlanc, F. Pérez-Rodríguez, S. Savel'ev, I. Voloshin, and V. Yampol'skii, "Suppression of the magnetic moment under the action of a transverse magnetic field in hard superconductors," Physical Review B **61**, 15382 (2000).
[27] J. R. Clem, "Flux-line-cutting losses in type-slowromancapii@ superconductors," Physical Review B **26**, 2463 (1982).
[28] J. R. Clem, M. Weigand, J. Durrell, and A. Campbell, "Theory and experiment testing flux-line cutting physics," Superconductor Science and Technology **24**, 062002 (2011).
[29] A. Campbell, "Flux cutting in superconductors," Superconductor Science and Technology **24**, 091001 (2011).
[30] J. Yoo and D. Youm, "Tensile stress effects on critical current densities of coated conductors," Superconductor Science and Technology **14**, 109 (2001).

[31]C. Park, D. Norton, J. Budai, D. Christen, D. Verebelyi, R. Feenstra, D. Lee, A. Goyal, D. Kroeger, and M. Paranthaman, "Bend strain tolerance of critical currents for yba_2 cu_3o_7 films deposited on rolled-textured (001) ni," Applied physics letters **73**, 1904–1906 (1998).

[32]H.-S. Shin, K.-H. Kim, J. R. C. Dizon, T.-Y. Kim, R.-K. Ko, and S.-S. Oh, "The strain effect on critical current in ybco coated conductors with different stabilizing layers," Superconductor Science and Technology **18**, S364 (2005).

[33]Superpower-inc.com, "Superpower-inc.com, (2014). 2g hts wire." (2014).

[34]R. Champailler, N. Yanagi, G. Bansal, H. Tamura, T. Mito, S. Imagawa, and J.-L. Duchateau, "Experiments of bending strain on reduced-scale hts conductors for fusion energy reactors," Applied Superconductivity, IEEE Transactions on **20**, 1565–1568 (2010).

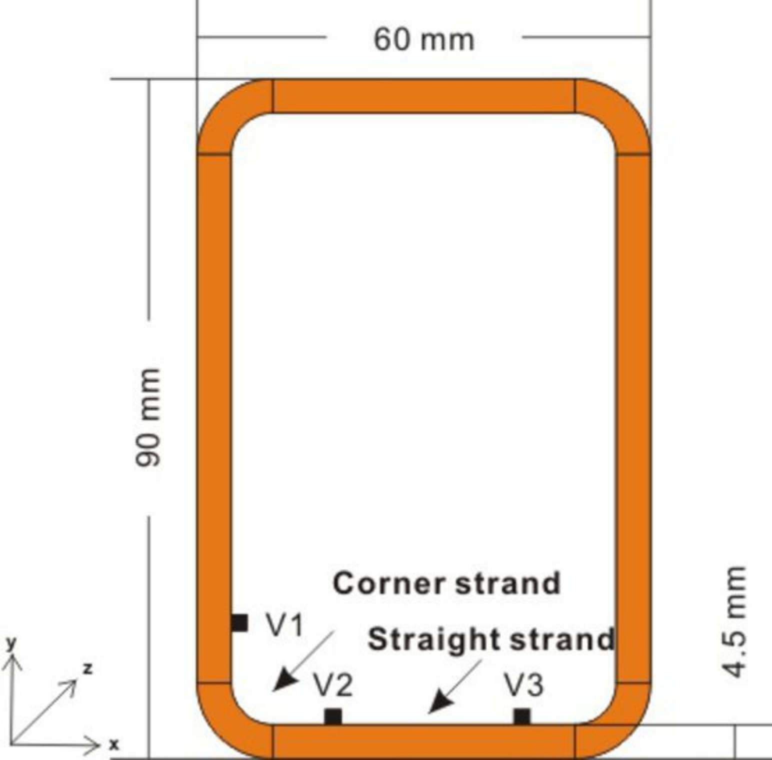

60 mm
90 mm
Corner strand
Straight strand
V1
V2
V3
4.5 mm
y
z
x

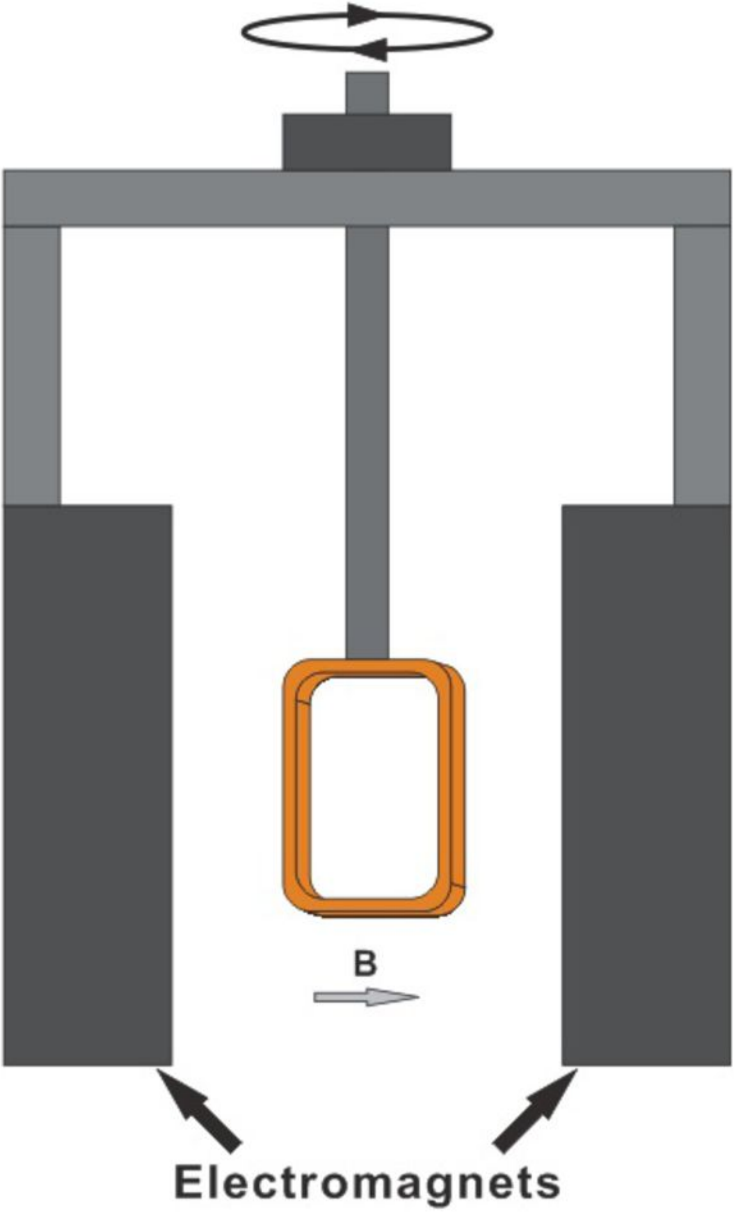
B
Electromagnets

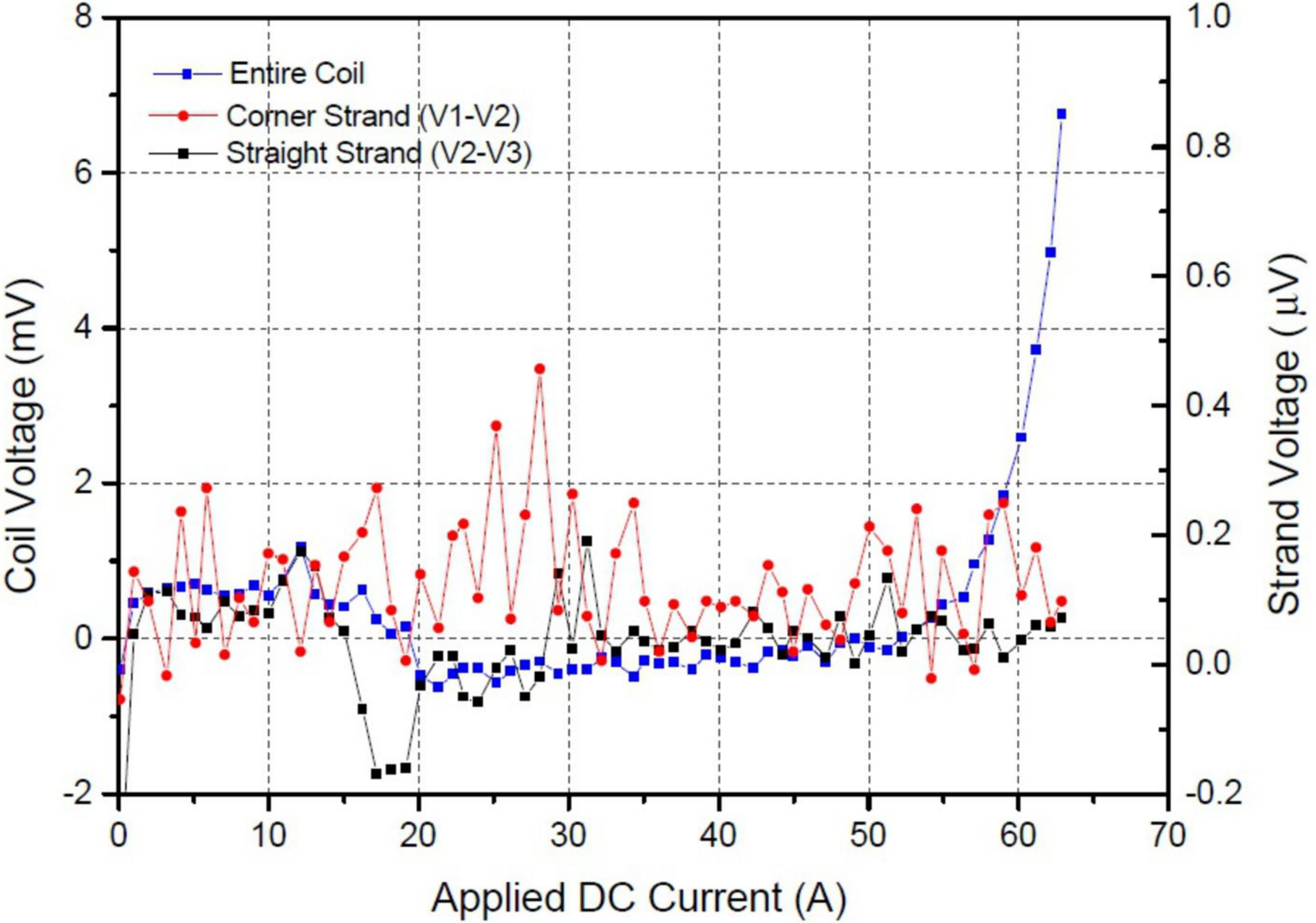

Entire Coil
Corner Strand (V1-V2)
Straight Strand (V2-V3)
Coil Voltage (mV)
Strand Voltage (μV)
Applied DC Current (A)
8
6
4
2
0
-2
1.0
0.8
0.6
0.4
0.2
0.0
-0.2
0
10
20
30
40
50
60
70

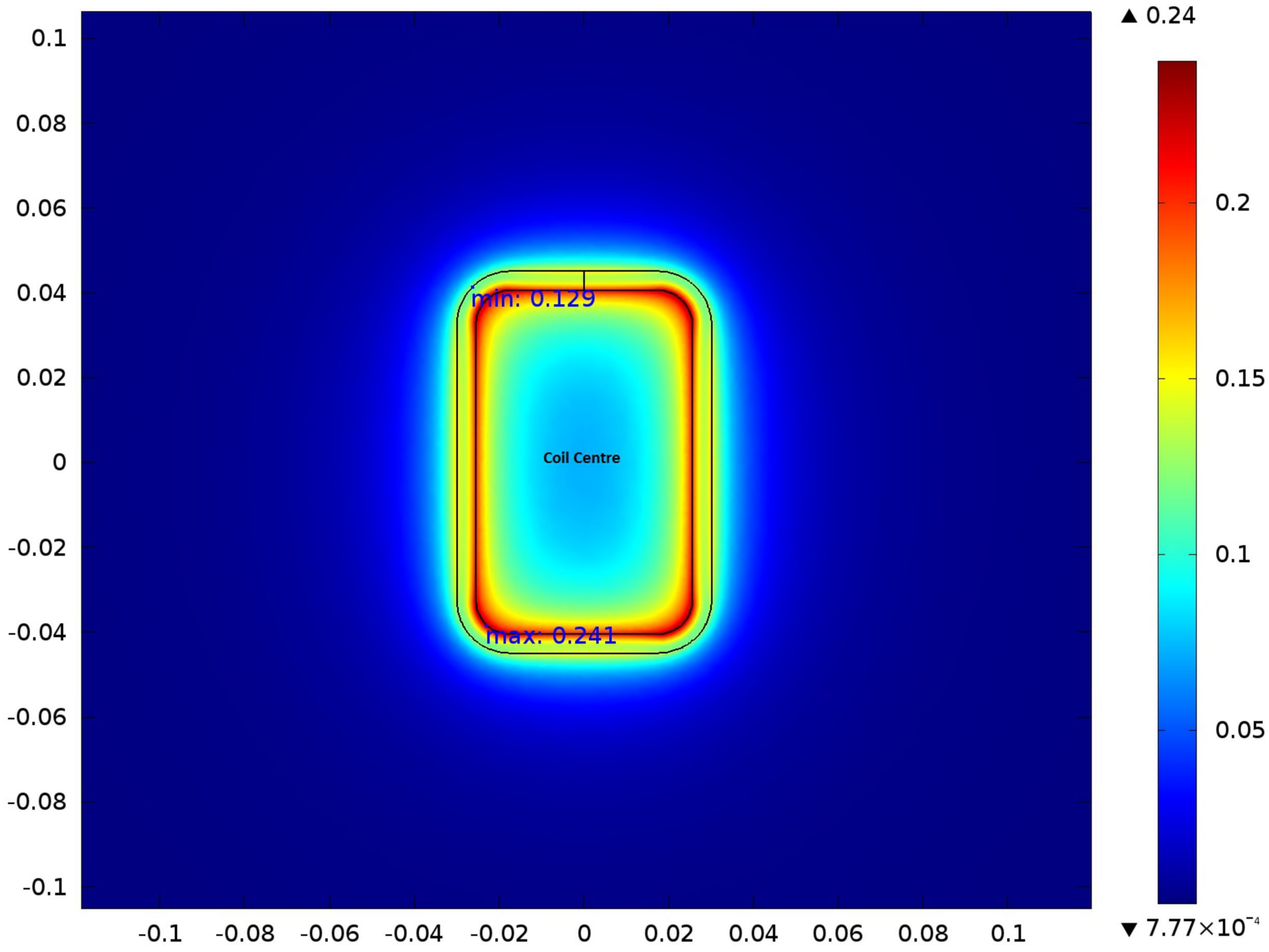

min: 0.129
max: 0.241
Coil Centre
0.1
0.08
0.06
0.04
0.02
0
-0.02
-0.04
-0.06
-0.08
-0.1
-0.1
-0.08
-0.06
-0.04
-0.02
0
0.02
0.04
0.06
0.08
0.1
▲ 0.24
0.2
0.15
0.1
0.05
▼ 7.77×10⁻⁴

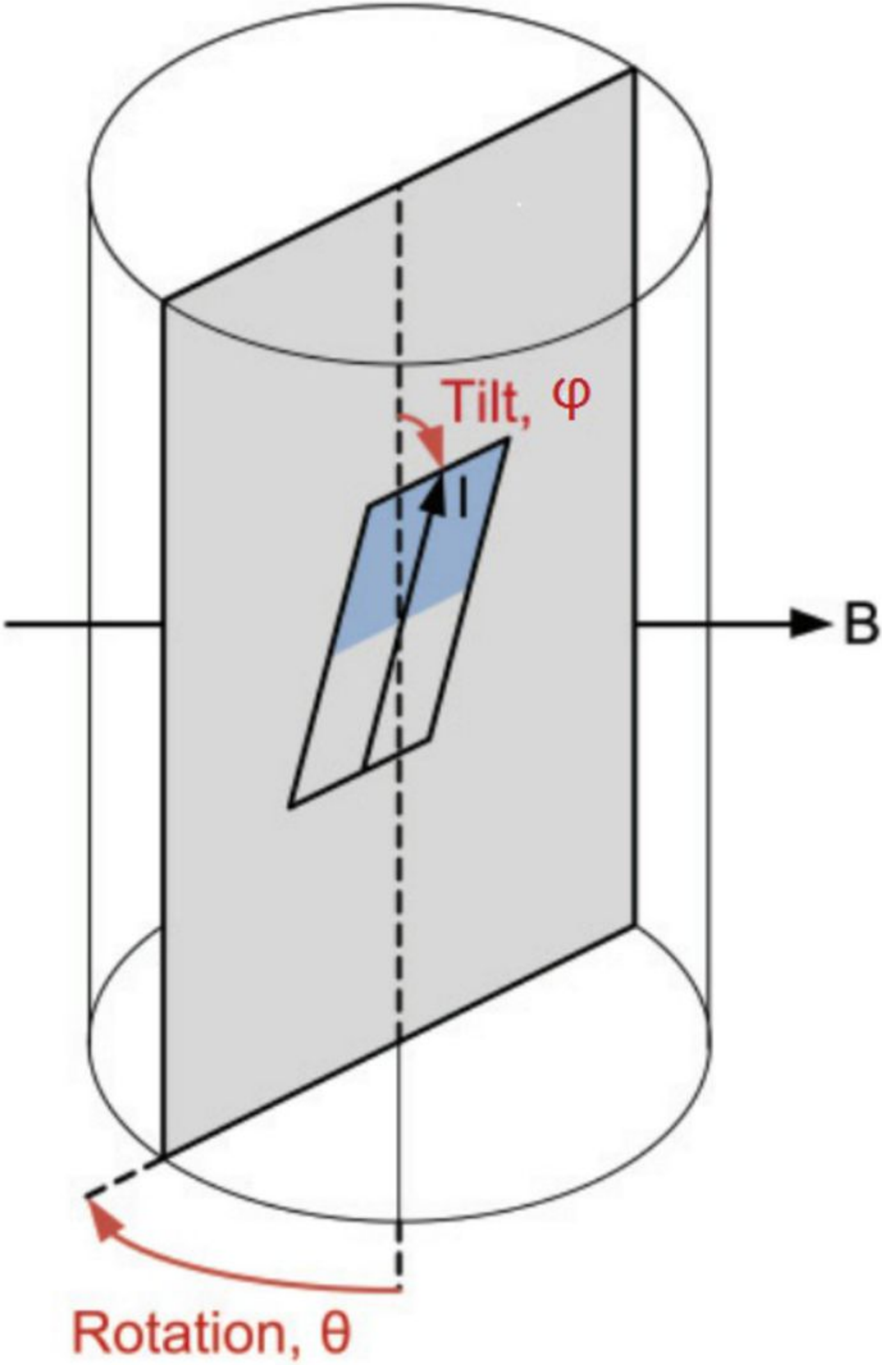

Tilt, φ
I
B
Rotation, θ

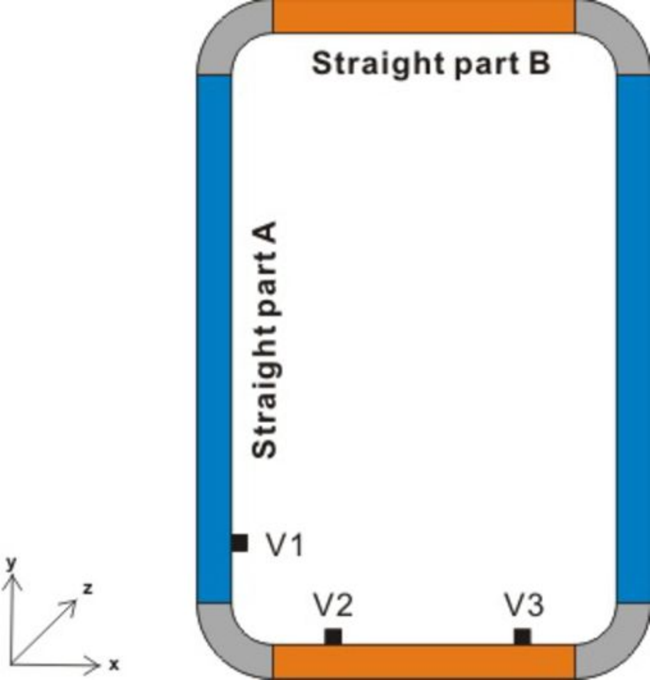

Straight part B
Straight part A
V1
V2
V3
y
z
x

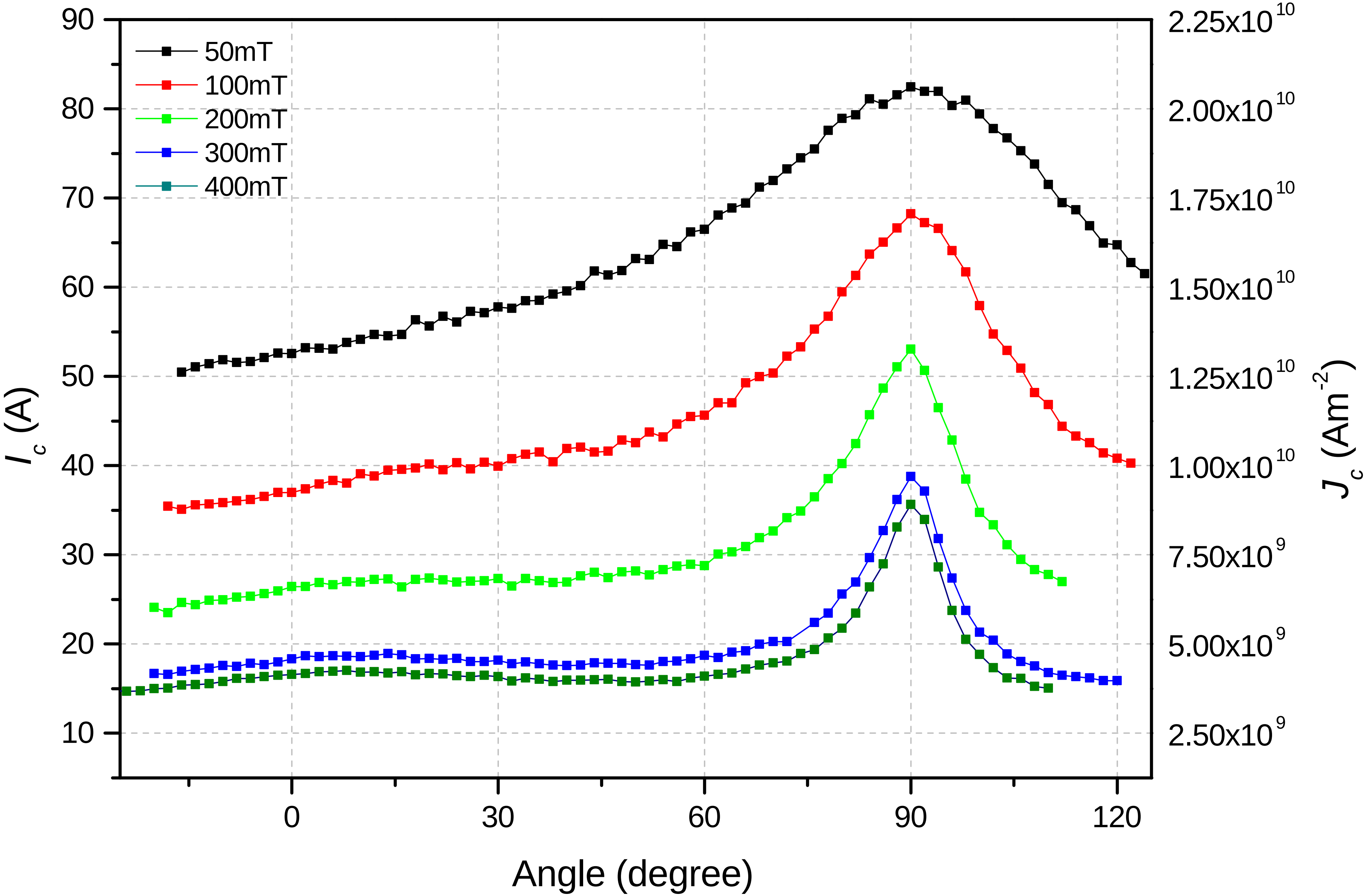

50mT
100mT
200mT
300mT
400mT
I_c (A)
J_c (Am^{-2})
Angle (degree)
90
80
70
60
50
40
30
20
10
0
30
60
90
120
2.25x10^{10}
2.00x10^{10}
1.75x10^{10}
1.50x10^{10}
1.25x10^{10}
1.00x10^{10}
7.50x10^{9}
5.00x10^{9}
2.50x10^{9}

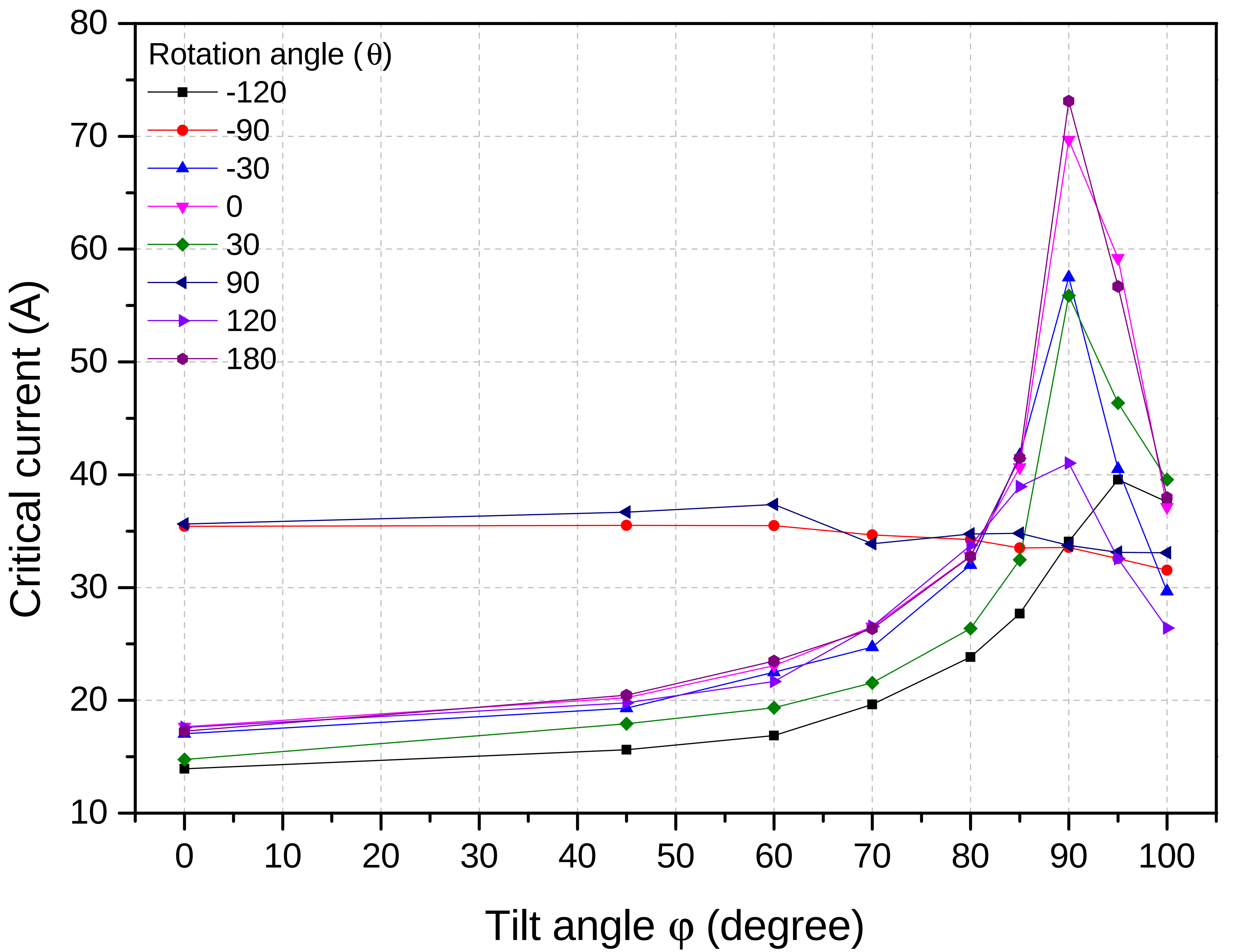

Rotation angle (θ)
-120
-90
-30
0
30
90
120
180
Critical current (A)
Tilt angle φ (degree)
80
70
60
50
40
30
20
10
0
10
20
30
40
50
60
70
80
90
100

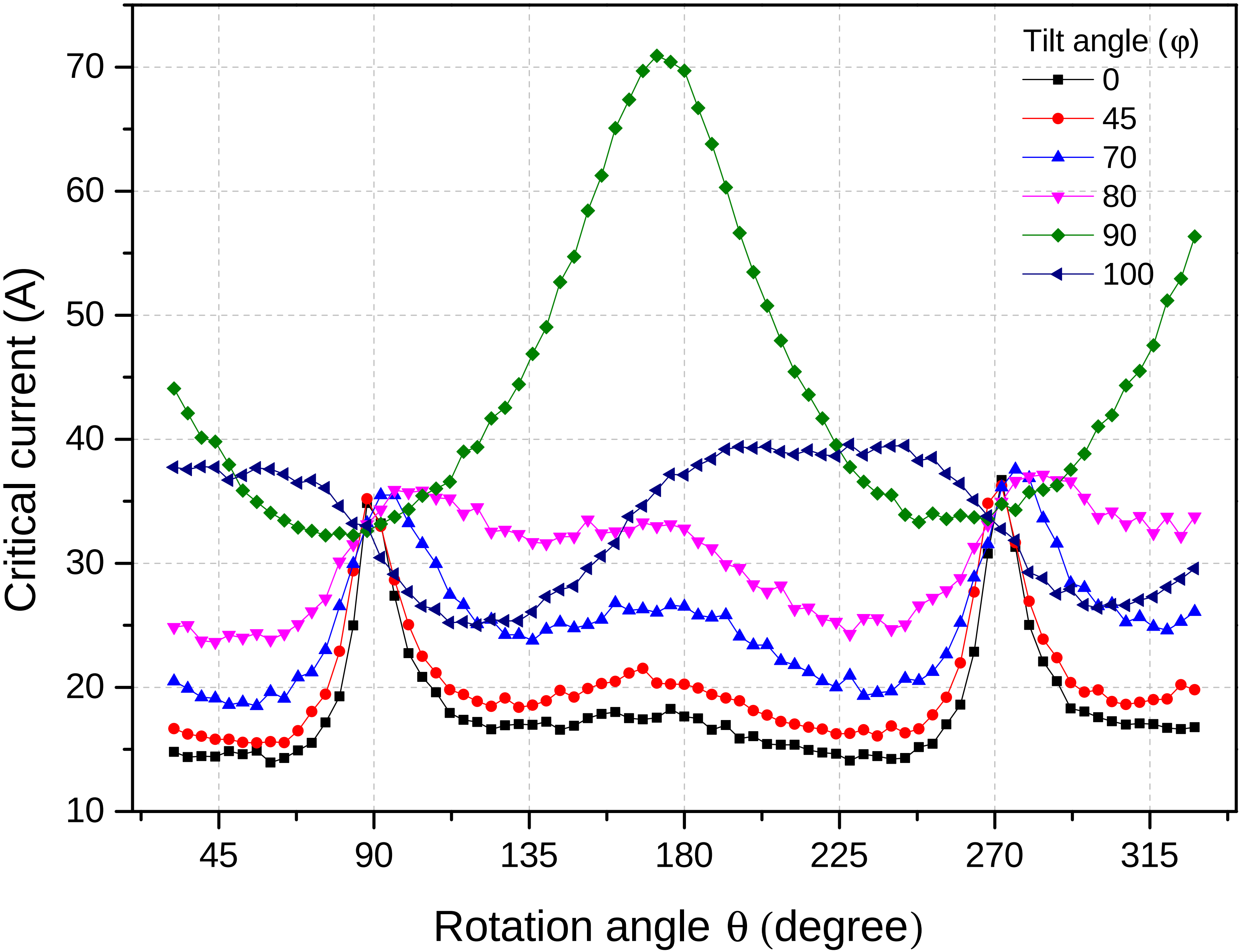

Critical current (A)
Rotation angle θ (degree)
Tilt angle (φ)
0
45
70
80
90
100
10
20
30
40
50
60
70
45
90
135
180
225
270
315

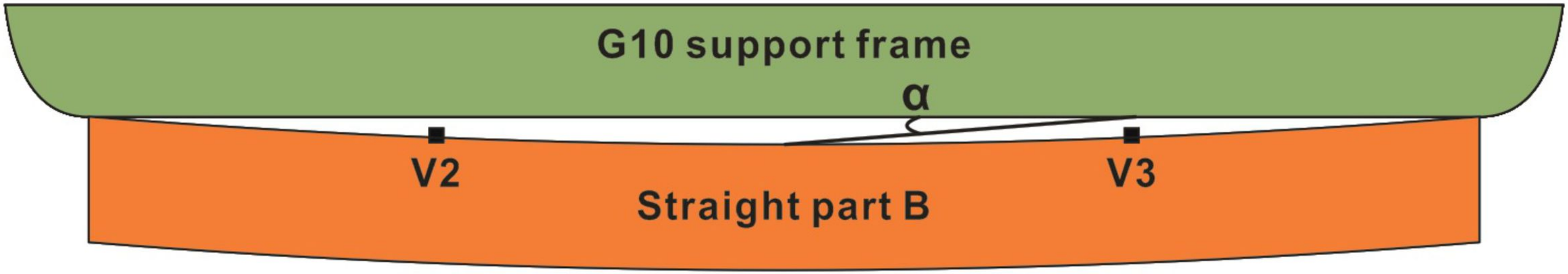
G10 support frame
α
V2
V3
Straight part B

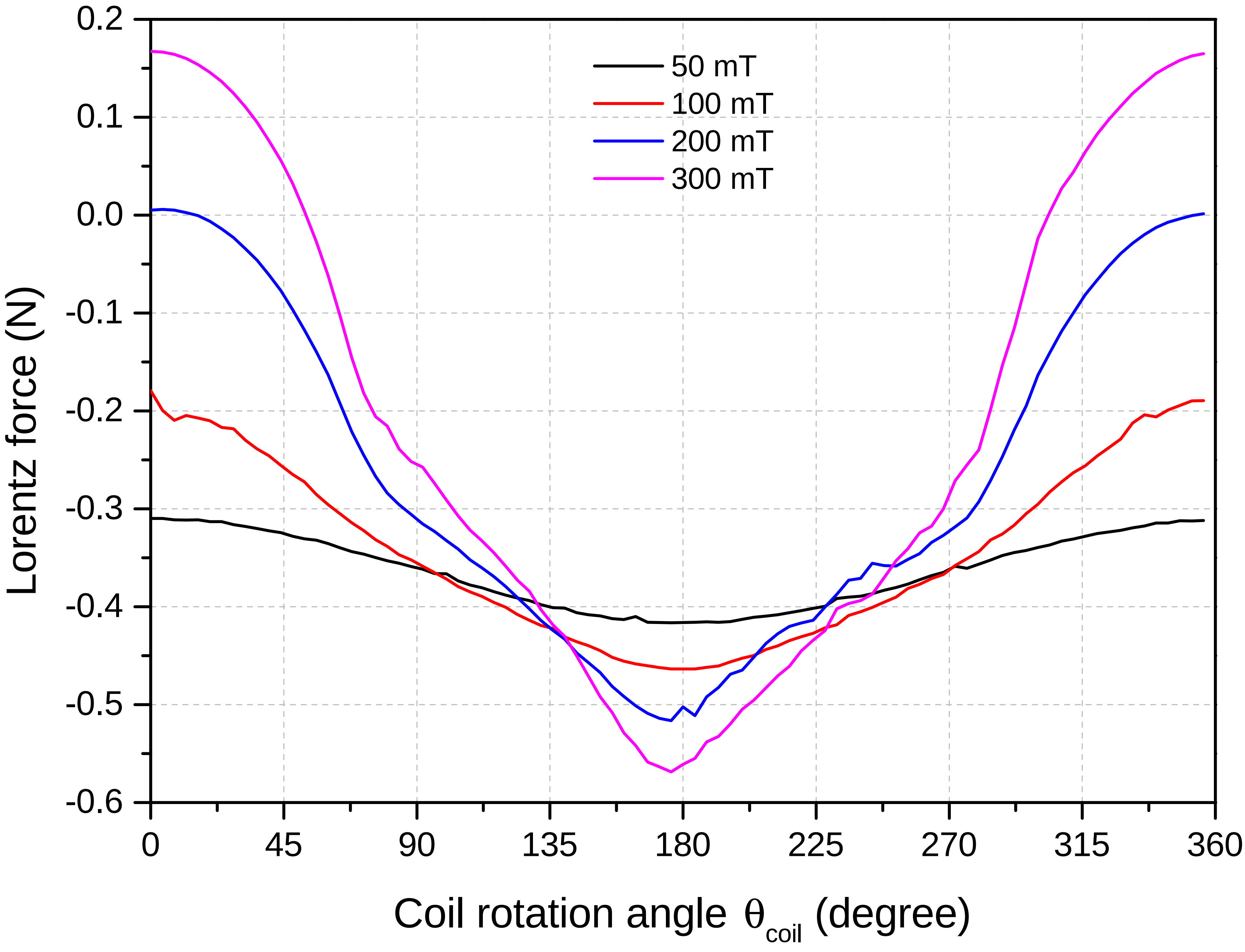
50 mT
100 mT
200 mT
300 mT
Lorentz force (N)
0.2
0.1
0.0
-0.1
-0.2
-0.3
-0.4
-0.5
-0.6
0
45
90
135
180
225
270
315
360
Coil rotation angle θcoil (degree)

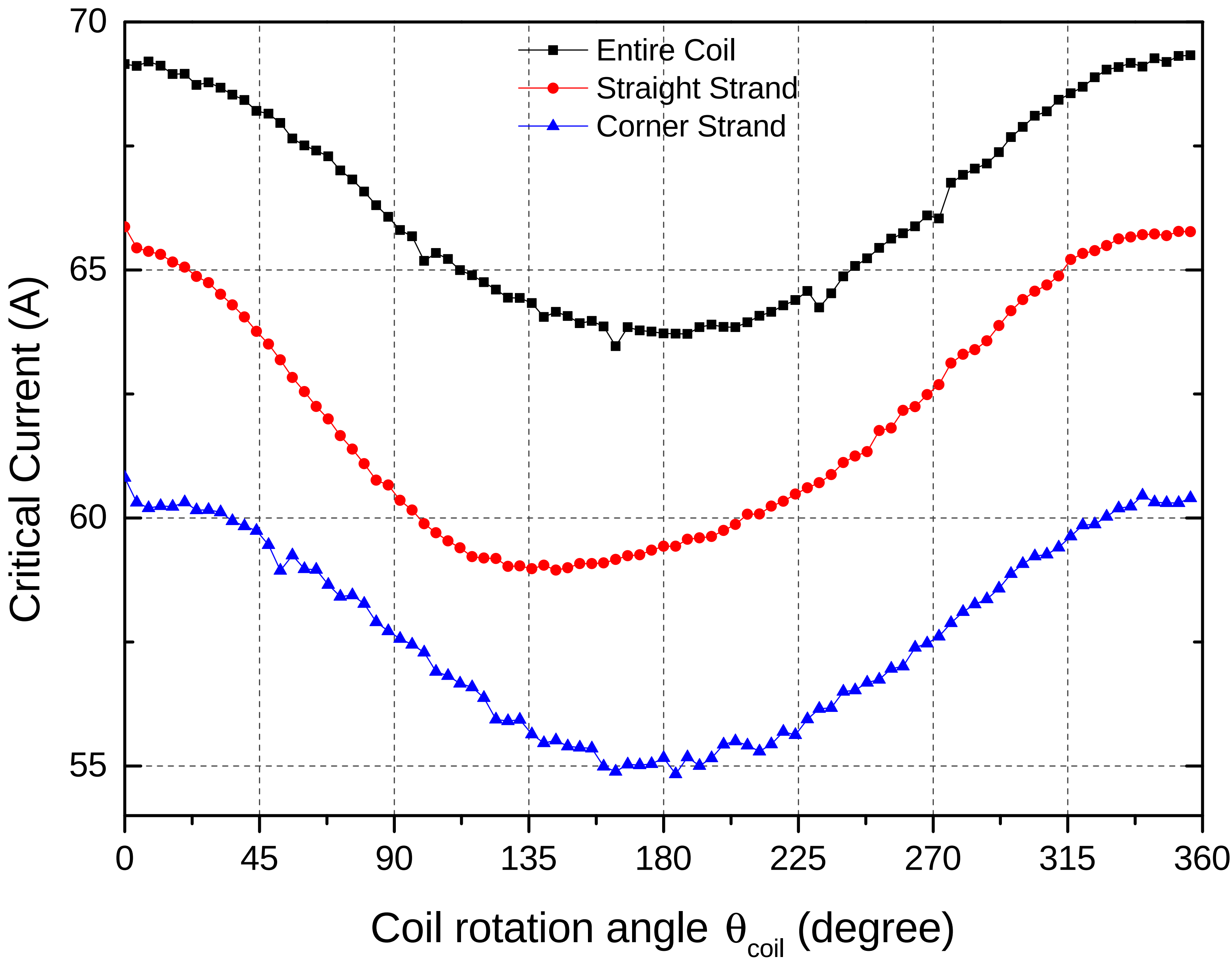

70
65
60
55
0
45
90
135
180
225
270
315
360
Entire Coil
Straight Strand
Corner Strand
Critical Current (A)
Coil rotation angle θ_{coil} (degree)

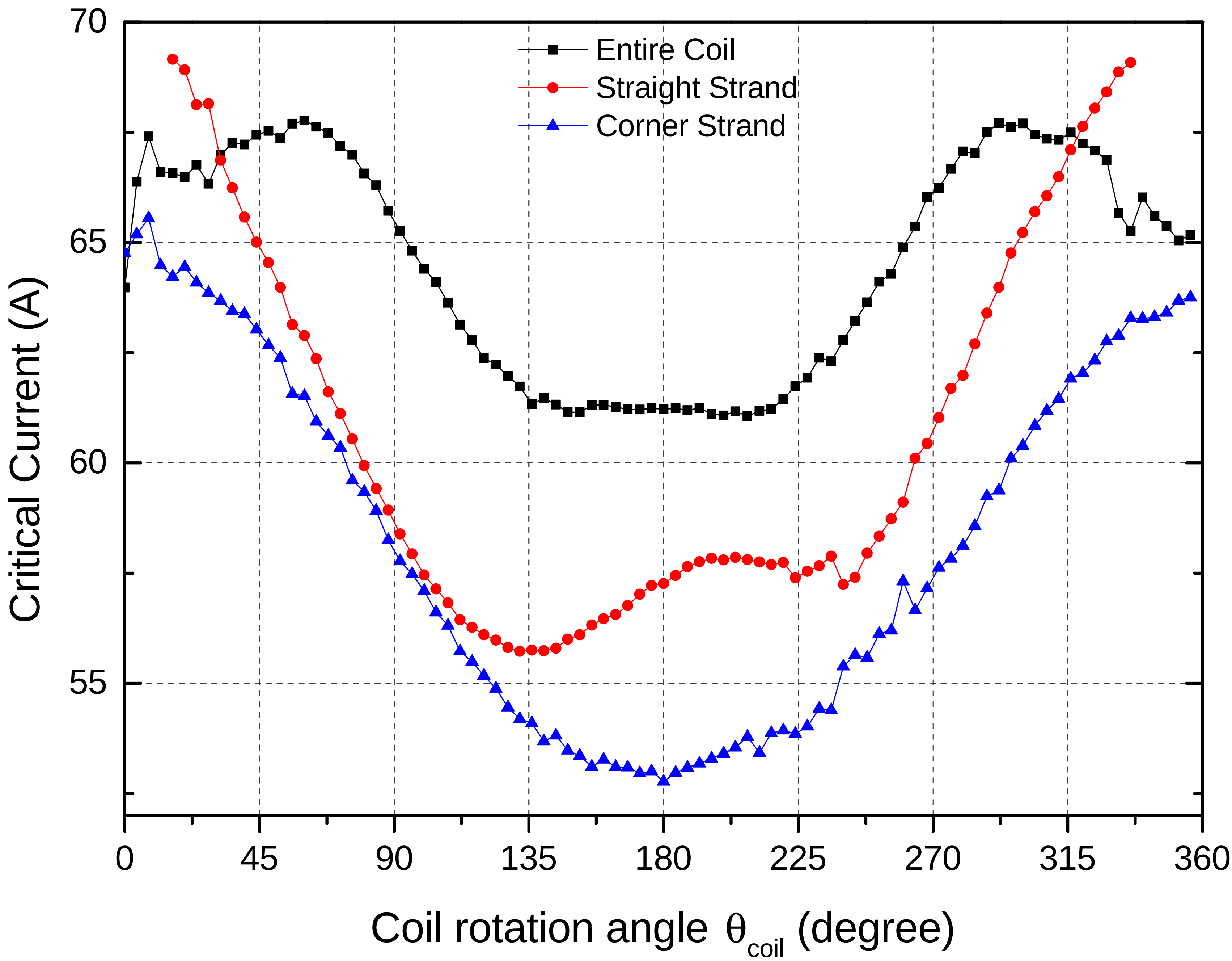

70
65
60
55
0
45
90
135
180
225
270
315
360
Critical Current (A)
Coil rotation angle θ_{coil} (degree)
Entire Coil
Straight Strand
Corner Strand

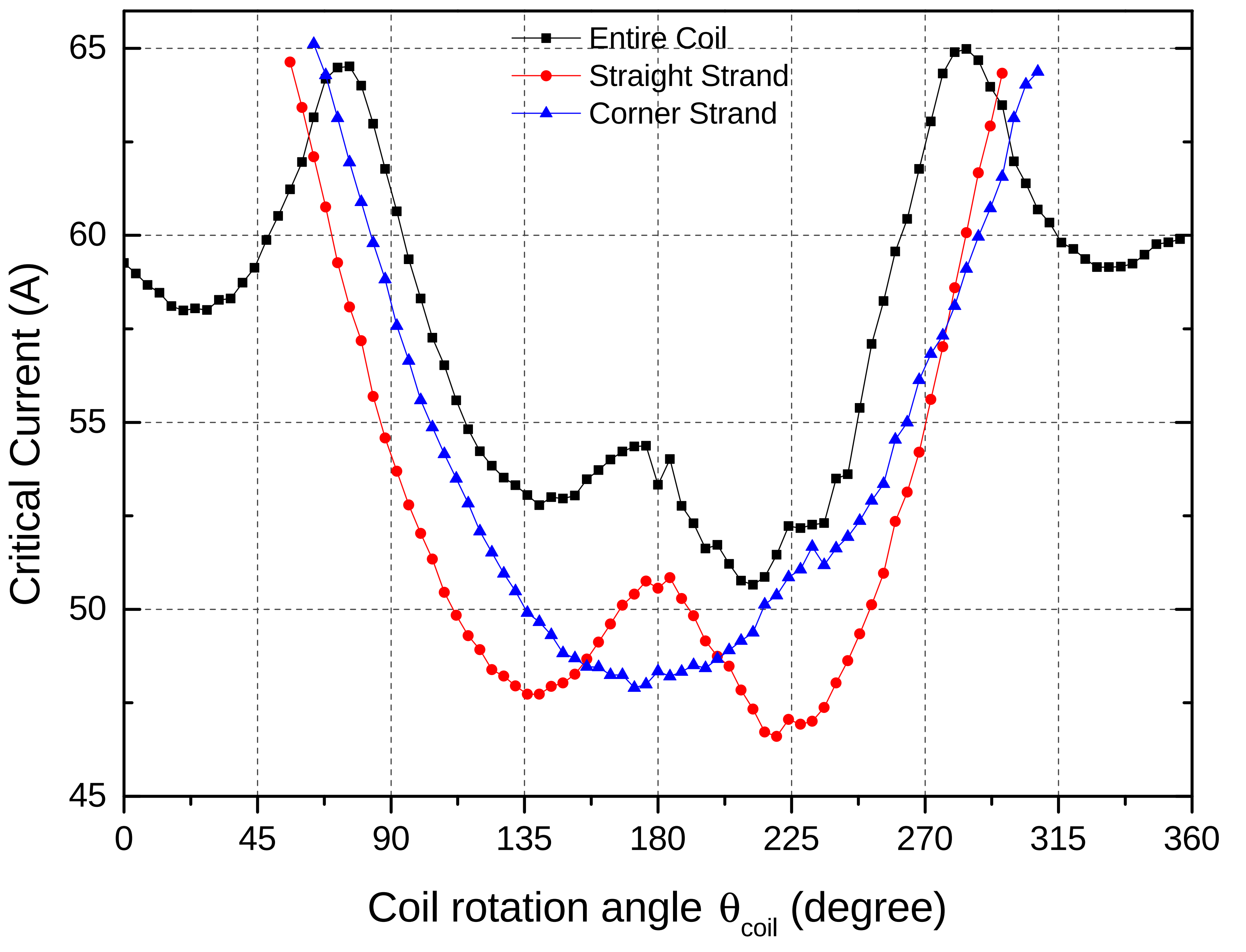
Entire Coil
Straight Strand
Corner Strand
65
60
55
50
45
0
45
90
135
180
225
270
315
360
Critical Current (A)
Coil rotation angle θ_{coil} (degree)

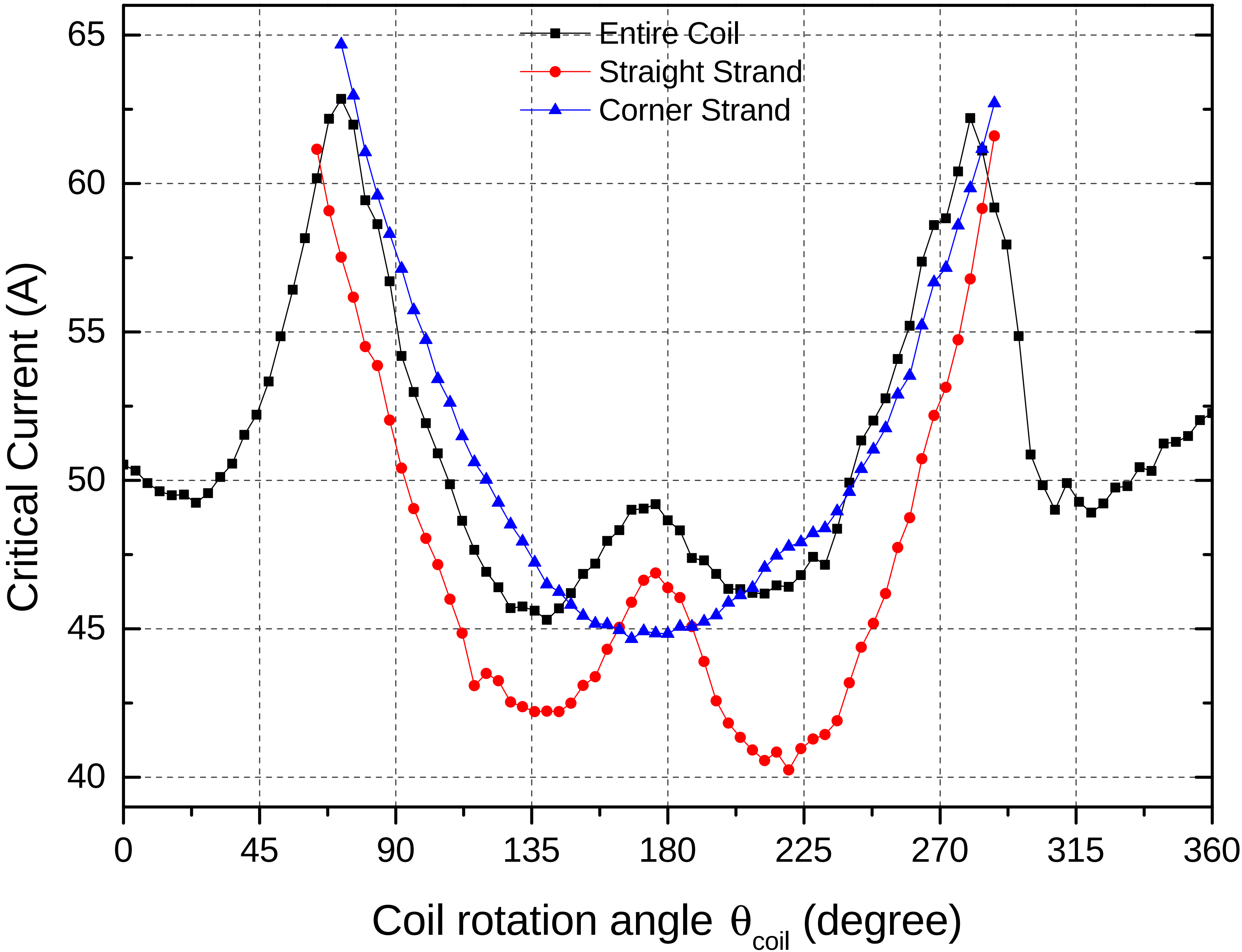

Entire Coil
Straight Strand
Corner Strand
Critical Current (A)
Coil rotation angle θ_{coil} (degree)
65
60
55
50
45
40
0
45
90
135
180
225
270
315
360

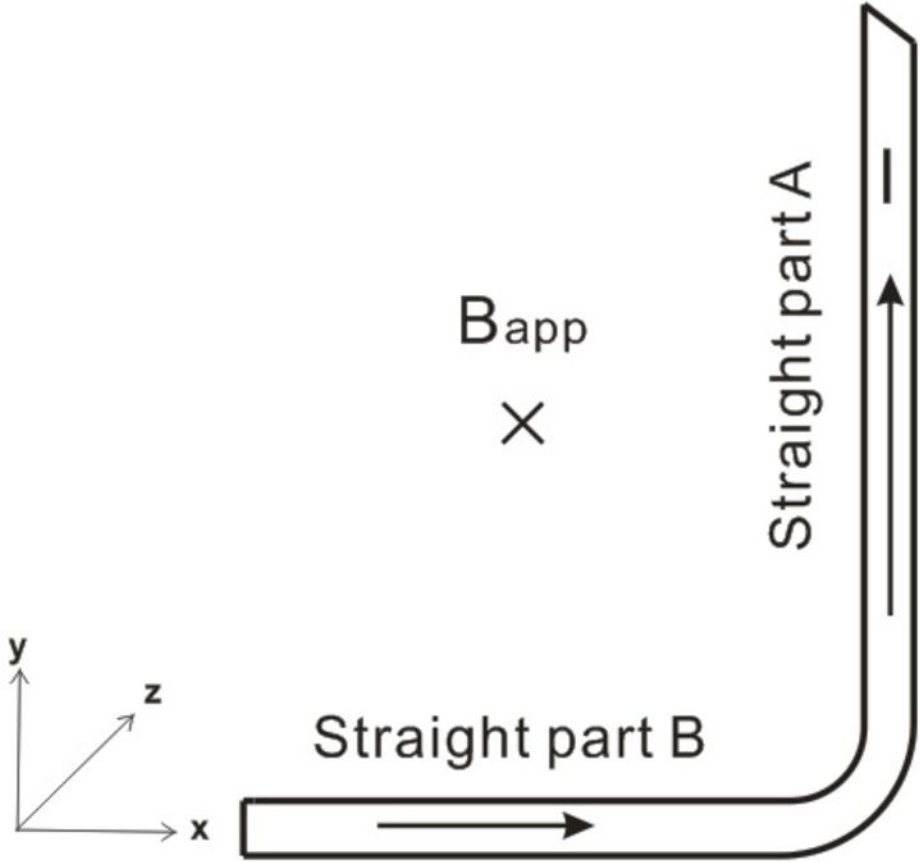
Straight part A
Bapp
Straight part B
y
z
x

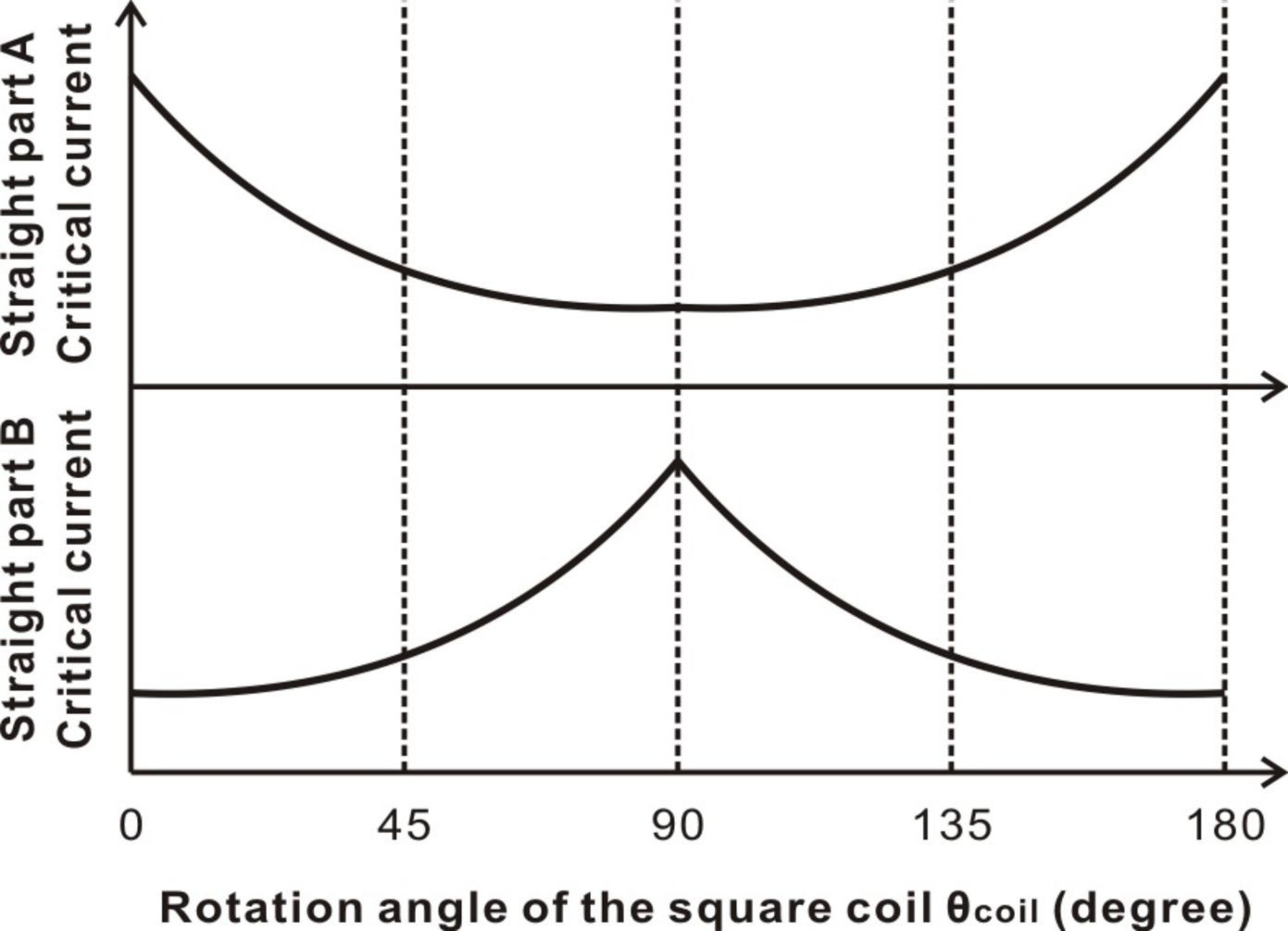
Straight part A
Critical current
Straight part B
Critical current
0
45
90
135
180
Rotation angle of the square coil θcoil (degree)

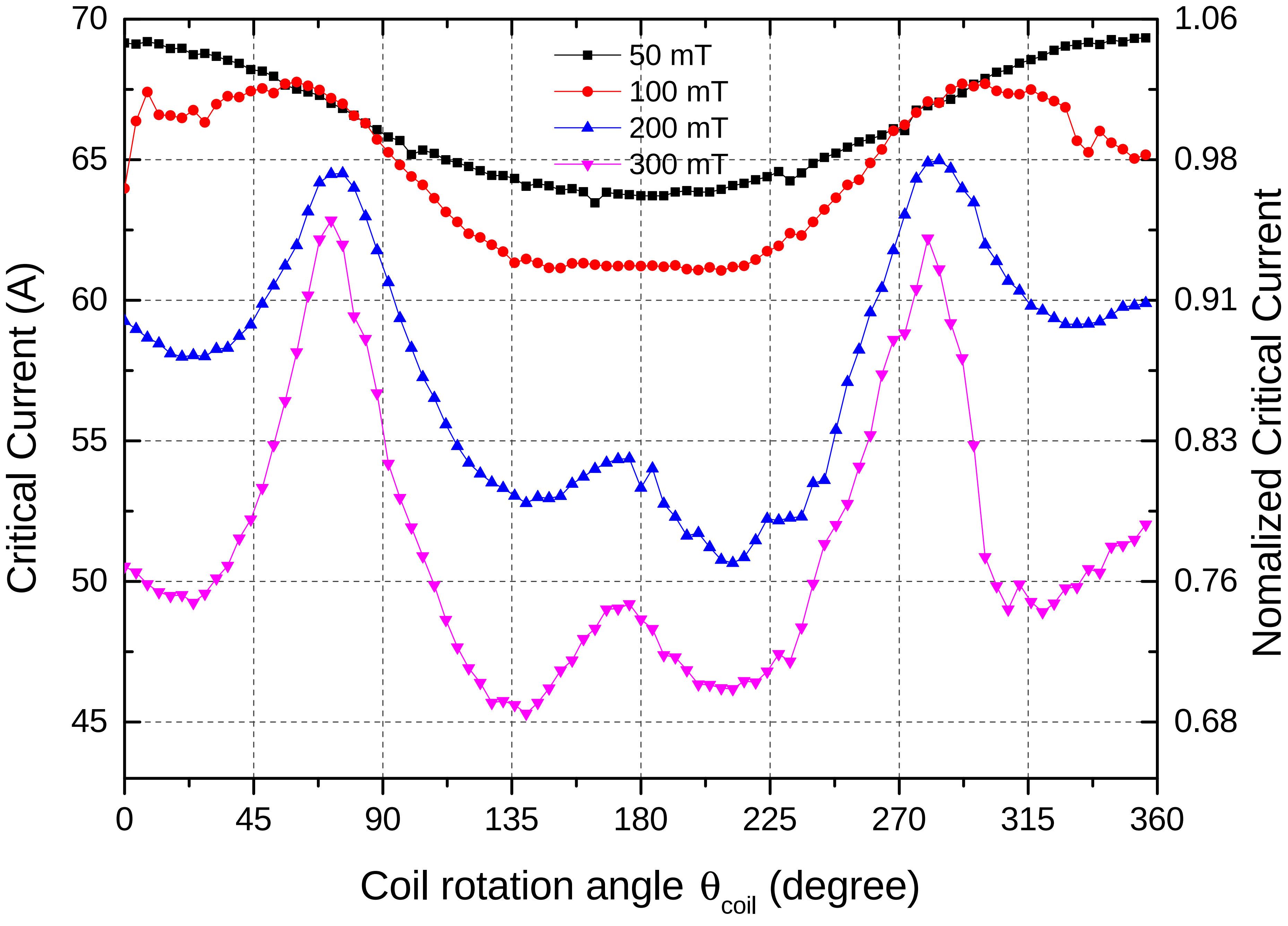

50 mT
100 mT
200 mT
300 mT
Critical Current (A)
Nomalized Critical Current
Coil rotation angle θ_{coil} (degree)
70
65
60
55
50
45
1.06
0.98
0.91
0.83
0.76
0.68
0
45
90
135
180
225
270
315
360